National Research Council Publication No. 2907
ISBN: 88-88885-04-8

Published by GRIFO Publishers, Perugia.
May, 2006

Advanced Specialisation
School And Research
Centre For The Maintenance
And Conservation
Of Historic Towns Built On Unstable Sites

National Research Council, Italy
National Group for Prevention from
Hydro-Geological Disaster

WARREDOC
Water Resources Research and
Documentation Centre, Perugia
University for Foreigners

International Hydrological
Programme (IHP)
Italian National Comittee

WATER FOR LIFE:
WATER RESOURCES AND RISK MANAGEMENT PERSPECTIVES

Edited by:

Kodwo Andah PhD
Scientific Coordinator, WARREDOC
Water Resources Research and Documentation Centre
University for Foreigners of Perugia, Italy

&
Marco Barluzzi
Vice Secretary General
Advanced Specialisation School and Research Centre
for the Maintenance and Conservation of
Historic Towns on Unstable Sites, Casalina (PG), Italy

Proceedings of the 1st Seminar of the Italian National Committee of IHP-UNESCO under the 2005-2015 United Nations Decade for Action "Water for Life"

Grifo Publishers

Perugia, 2006

CNR - GNDCI
Pubblication N° 2907

The Use of Meteorological Radar in Flood Mitigation: Some Preliminary Results

Francesco Napolitano, Fabio Russo & Federico Lombardo
Department of Hydraulics, Highways and Roads, University of Rome "La Sapienza", Italy
(E-mail: francesco.napolitano@uniroma1.it; fabio.russo@uniroma1.it;
federico.lombardo@uniroma1.it)

Keywords: Rainfall fields, Weather radar, Flood forecasting, Rainfall stochastic model

Abstract:

Rainfields estimation over a catchment area is an important stage in many hydrological applications. In this context, weather radars have several advantages, since a single site is able to obtain coverage over a vast area with high temporal and spatial resolution. In this work, we investigated the areal reduction factor (ARF) by using radar reflectivity maps collected with the Polar 55C weather radar. Radar rainfall estimations were integrated for heavy rainfall with an upscaling process, until we had rainfall estimation over an area of 900 km^2. Results obtained for several rainfall events by using this technique are compared with the most important relations of ARF in literature. Furthermore, the calibration of the GDSTM model, a cluster stochastic generation model in continuous space and time, is hereby presented. For the validation of the ability of the model to reproduce internal structure of rain events, a geo-morphological rainfall-runoff model, based on width function, was calibrated using simulated and observed data.

1. Introduction

Hydrological formation, concentration and propagation processes of runoff into natural basins are strongly affected by heterogeneity in space and time of rainfall fields, Bras and Rodriguez-Iturbe (1976), Chua and Bras (1982), Bastin et al. (1984). In particular, for small and medium range basins, the extreme variability in space observed in rainfall fields consequently can often lead to evaluation errors as regards rainfalls and their respective simulated discharges, Todini (1995), Borga et al. (2000). A remarkable contribution to the elimination of these errors can be achieved by the estimation of rainfall fields starting from reflectivity maps collected by weather radars, Anagnostou and Krajewski (1999).

In order to realise effective and swift civil protection actions, it is crucial to produce in real time the possible development of a storm occurring in that moment. Towards this purpose, rainfall time series of possible events can be simulated, useful to assess the hydraulic risk for natural basins. This can be identified by using generated scenarios as an input to rainfall-runoff models. They are also useful for the evaluation of downpour risk in urban areas, and also for pursuing the best strategy for man-made works inside complex urban drainage systems.

Space and time stochastic precipitation models are, potentially, an instrument capable of meeting these needs. Austin and Houze (1972) identified some specific elements of rainfall fields in space by underlining the trend of rain cells to cluster inside larger-scale structures called "small mesoscale areas" (SMSA), contained inside large mesoscale areas (LMSA), which, in turn, are contained inside synoptic areas. On the basis of these observations, Northrop (1996) developed the GDSTM model (Gaussian Displacements Spatial-Temporal Model) by expanding in space single-site stochastic models used to represent the rainfall in time and at a single site, Waymire and Gupta (1981), Waymire et al. (1984), and by up-grading the simpler Cox and Isham space-time model (1988).

In order to calibrate the above-mentioned model and to later check it, it is necessary to avail oneself of the observed rain fields at a high spatial-temporal resolution rate. The availability of this information is guaranteed in the studied area by the Polar 55C weather radar. Due to this precipitation structure, it can be observed that both high intensity rainfall clustering in small areas and rainfall intensity decrease with increasing the distance from the point of highest rain intensity.
The reduction of high intensity rainfall with respect to vast areas is a key issue in many hydrological problems, e.g. in designing hydraulic structures for flood control, such as urban drainage systems, Bacchi and Ranzi (1996). As a solution of this problem the Natural Environmental Research Council (NERC) Flood Studies Report, NERC (1975) introduced the areal reduction factor (ARF) defined as the factor which has to be applied to point rainfall measurements for specified duration and return period in order to obtain areal rainfall for the same duration and return period. In this work, we investigated on the ARF by using Polar 55C reflectivity maps.
The present paper is developed as follows: first, an overview of the Polar 55C weather radar is given. Second, the GDSTM model is described, calibrated, checked and used in a case study of flood forecasting. Third, the methodology in calculating the ARF is explained and results are shown. Finally, all results are discussed.

2. The weather radar

The weather radar is an electronic device which is capable of detecting hydrometeors (raindrops) by transmitting an electromagnetic signal into space, and receiving back echoes from those targets, Rinehart (1991). The Polar 55C is a C-band (5.5 GHz, $\lambda = 5.4$ cm) Doppler coherent weather radar with polarization agility and with a 0.9° beamwidth, managed by the Institute of Atmospheric Sciences and Climate of the National Research Council. The C-band is a good compromise between the accuracy in the rain-measuring and problems due to the antenna dimensions. Also, in this scheme, the radar is able to transmit and to receive horizontally and vertically polarized signals on alternate pulses, allowing us to measure not only the most used horizontally reflectivity factor (Z_h), but also the differential reflectivity (Z_{dr}) and the differential phase shift (Φ_{dp}). Radar measurements are obtained by averaging 64 pulses with a range-bin resolution of 75 m, up to 120 km away from the radar location. A radar image is available every five minutes.
Preliminary analyses on plan position indicators (PPI) collected at different elevations were performed in order to find the best antenna elevation for radar rainfall estimation. The radar operational elevation angle is obtained by minimizing both ground-clutter and melting layer contamination. Furthermore, reflectivity maps were adequately corrected by filtering out all of the ground-clutters by using a specific algorithm based upon the backscattering signal variance of the differential reflectivity, Gorgucci et al. (1995), Russo et al. (2005). Figure 1 shows a radar reflectivity map where the beam blockage phenomenon is evident in the South-Eastern region, caused by the Cavo mountain, located near the radar.
In order to convert observed reflectivity into rainfall intensities, an algorithm based on a Z-R relation is used. This relation was obtained for C-band by means of a non-linear regression analysis, Russo et al. (2005):

$$R = 7.27 \cdot 10^{-2} Z_h^{0.62} \quad (1)$$

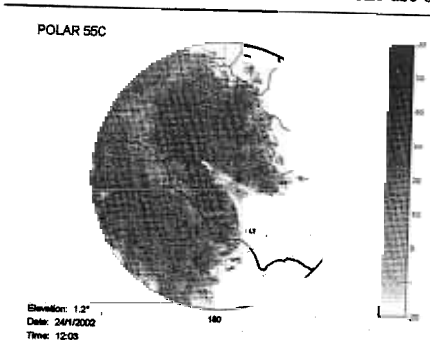

Figure 1. A reflectivity map (PPI) collected by the Polar 55C weather radar on 24th January, 2002

3. The "GDSTM" spatial–temporal model

The model described hereunder, proposed by Northrop (1996), is characterised by a more accurate physical interpretation than that provided by previous models. The mathematical description is more complicated and it requires more time to calculate its implementation.
The following are the basic hypotheses of the model:

- within a rain event, storm centres arrive according to a homogeneous Poisson process with λ rate in bi-dimensional space and in time; inside each storm, cells arrive, in respect of the storm centre, according to a Bartlett-Lewis process with β rate;
- the cell-generating process ends after a period of time exponentially distributed with γ parameter; the number of cells per storm C has, therefore, a geometric distribution with mean $\mu_C = 1 + \beta/\gamma$; each cell within the storm is displaced from the storm centre by a vector which is drawn independently from a bivariate Gaussian distribution with mean 0 and co-variance matrix Σ. The Σ elements vary from storm to storm, in a way to change the storm areas. In fact, the values of σ^2_x are independent random variables in function of a ς parameter and of inverse χ-square distribution with ψ degrees of freedom, and σ^2_y, in turn, is function of σ^2_x;
- each rain cell has an elliptical shape with major axis with a random length A_C distributed according to Γ distribution with α_1 e α_2 parameters, and has a constant rainfall rate (X distributed according to an exponential distribution with χ parameter) all over, with a D duration distributed according to an exponential distribution with η parameter;
- each rain cell has the same E eccentricity and Θ orientation of the storm. In this way E and Θ are fixed data, given the Σ;
- the variables A_C, D and X are mutually independent among cells and independent of Σ; the storm centre and the cells, belonging to it, travel at the same speed $V = (V_x, V_y)$: so all cells develop inside the storm e and the shape of the storm does not change during the travelling;
- cell clusters belonging to distinct storms are independent.

The GDSTM model has therefore 13 parameters. For further information on the model see Northrop's work (1996).

3.1. Model fitting

Model fitting is based upon the method of moments proposed by Hansen (1982). An objective function, represented by the weighted sum of squared differences between a set of n theoretical and observed values, is numerically minimised with respect to the model parameters.
If ω denotes the p×1 vector of parameters of the model, $Z^{(m)}{}_1(\omega)\ldots Z^{(m)}{}_n(\omega)$ denote the model values of selected properties and $Z^{(o)}{}_1(\omega)\ldots Z^{(o)}{}_n(\omega)$ denote the corresponding observed values, the objective function is given by:

$$\min_{\omega} \sum_{i=1}^{n} \left(\frac{Z_i^{(m)}(\omega) - Z_i^{(o)}}{w_i} \right)^2 \quad (2)$$

where n = p is assumed.

The vector of weights is set $\{w_i\} = 1$ because the absolute error is not supposed to depend on the magnitude of the properties involved, Northrop (1996).

The choice of the fitting properties is based on the following criteria:

- statistical properties chosen must not be related to each other in a significant way;
- the evaluation of theoretical values must not be computationally too expensive.

The following are the 13 properties used for the estimation of the 13 parameters of the model:

- mean;
- variance at three levels of spatial aggregation;
- temporal autocorrelation $\rho(0,t)$ at 2 time lags;
- spatial autocorrelation $\rho(\hat{u},0)$ at 5 space lags;
- two space-time cross-correlations.

3.2. Calibration of the model on Rome's area

In order to calibrate the above-mentioned model and to later check it, a square region (132 km x 132 km), centred in respect of the radar, is considered as to characterise the spatial-temporal evolution of a rain event both in the urban area of Rome and on the hydrographical basins in the outskirts of Rome (up to 80-90 km). Figure 2 allows to focus on the case-study region with respect to the radar location, to the city ring road, to the coast-line and to the hydrographical network of the Tiber river.

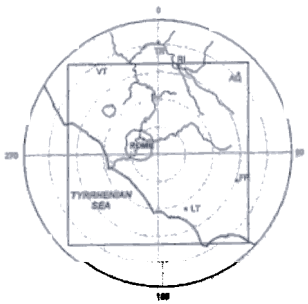

Figure 2. Study area 132 km x 132 km, shown against the radar scanning range and the main geographical reference points

3.3. Checking the model

In order to check the model, 50 scenarios, related to the possible evolution of the rain event observed in the whole area, were simulated for a minimum of three hours and a maximum of six hours.

The evolution scenarios of the precipitation process, produced by GDSTM, were compared to those actually recorded through the weather radar. In particular, in Figure 3, one image of the observed field and the corresponding simulated one are shown.

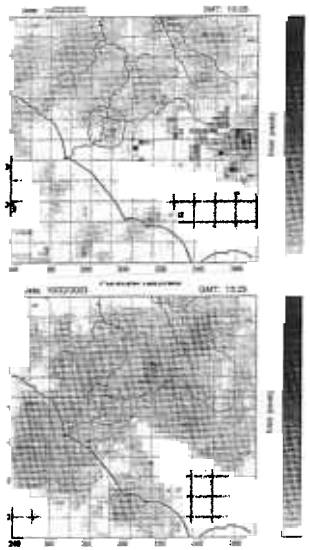

Figure 3. Observed rainfall field and the relevant forecast on 22nd October, 2003

In Figure 4, the rain intensity and the cumulative depth trends are reported. They are averaged over the study area for observed and simulated values of the event of 22nd October, 2003.

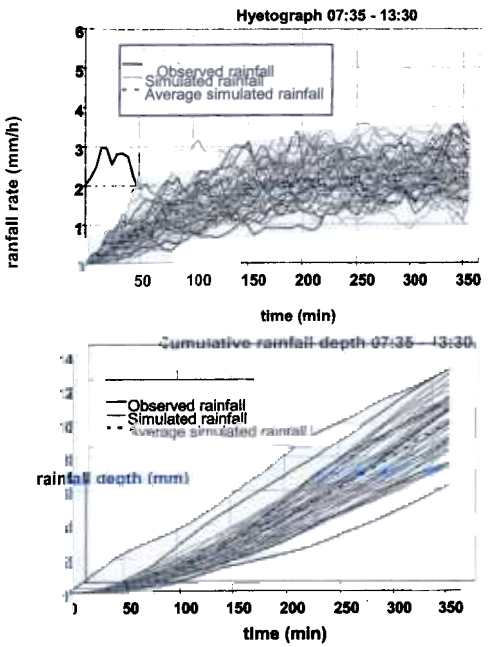

Figure 4. Rain intensity and cumulative rain depth, average over the study area, observed and simulated for the rain event on 22nd October, 2003.

The scenarios produced in the simulation show a transitory stage going from a 0 value to the average value of rain intensity. This transitory range lasts about three hours. In particular, the presence of the transitory range – during which the simulated fields underestimate the rainfall intensity – leads to a clear underestimation of the cumulative rain depth, mean over the area, simulated vis-à-vis the observed values.

3.4. Flood forecasting

In order to check the ability of the GDSTM model to provide realistic rainfall scenarios for flood forecasting, simulated rainfields were used as an input of a geo-morphological rainfall-runoff model based on width function (WFIUH). This model is calibrated for the Treia river basin, Lopez et al. (2005). The basin outlet is about 50 km away from the Polar 55C, with a catchment area of about 470 km^2. Figure 5 shows that the whole basin is within our study area.

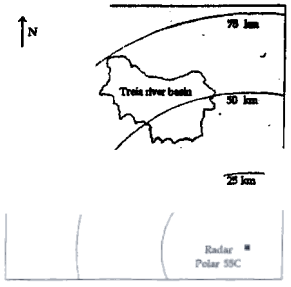

Figure 5. Location of the Treia river basin against the radar one.

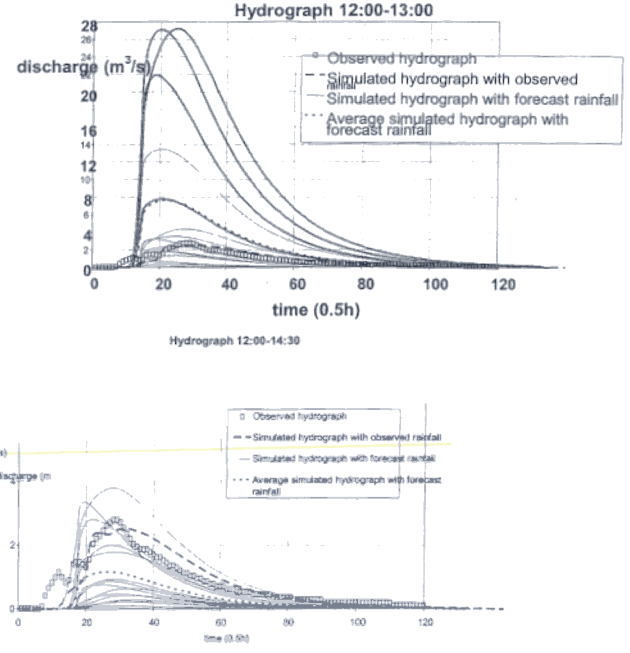

Figure 6. Observed and simulated discharges.

In Figure 6, it is possible to observe that the hydrograph recorded by the stream-flow gauging station (located near the basin outlet) and the ones simulated by the model, using rainfields estimated by the radar as an input, are very close together. The rainfall-runoff model does not therefore introduce significant errors in simulating discharges using GDSTM's rainfields as an input.

Besides, in order to check the model the rain event of the 24th January, 2002 was chosen and 15 4-hour rainfall scenarios were simulated for the observation ranges 12:00-13:00 and 12:00-14:30 a.m., which were used as an input to the rainfall-runoff model. Some results are shown in Figure 6. In either case, heterogeneity of simulated rainfields has strong repercussions on discharge estimates.

4. Areal reduction factor

The aim of our work is that of analysing the ARF trend when increasing the area at different durations and return periods. Mathematically, the ARF is non dimensional and can be expressed as follows:

$$ARF(\delta,T)=\frac{i_A(\delta,T)}{i(\delta,T)} \qquad (3)$$

where δ is the duration, T is the return period, the numerator and denominator of the right term represent the areal and point rainfall rate respectively. In our work, the rain rate observed by a raingauge is supposed to be quite similar to the rain rate estimated by the radar over a 1 km x 1 km region. Consequently the point rainfall rate is given by:

$$i(\delta,T)=i_{A=1}(\delta,T) \qquad (4)$$

On the basis of these considerations, the entire radar scanning field was discretized by a grid with 1 km x 1 km pixel. The rainfall intensity over each pixel – per each PPI of each event considered – is calculated as follows:

- evaluation of the total range-bin number which falls within the pixel considered;
- evaluation of the range-bin number with a valid value – i.e., a value which is recognized to be a real rainfall datum by the ground-clutter removal algorithm, Russo et al. (2005) – which falls within the pixel considered;
- in order to make the rainfall measurement meaningful for a pixel, we have assumed a threshold so that the number of valid range-bins must be at least equal to 25% of the total number of range-bins which fall within the same pixel;
- if the above condition proves valid, the rainfall intensity over the pixel is calculated by averaging the rainfall intensity values of all valid range-bins. Otherwise, the value of -99 (no-data) is given to the pixel.

In order to estimate the rainfall intensity at selected durations (δ = 1, 5, 10, 60, 120 min), we assumed that the rainfall intensity of a single radar image lasts one minute. Therefore, this is the minimum time resolution used. This hypothesis is based upon the fact that the time necessary for the antenna to record an entire PPI – which would give the information about the whole observation area – lasts about one minute (~ 55 s). Thus, the utmost temporal resolution available is equal to 1 PPI per minute and this is due to technical shortcomings.

For higher temporal aggregations, a vector with time intervals between consecutive PPIs is built. If time intervals are longer than 7 minutes, the value of -99 is given for the corresponding element of the vector with the aim of identifying possible malfunctioning and interruptions in radar recording.

A "time mobile window" – which is as large as the temporal aggregation to be studied – scans in time the entire rain event for each pixel of the grid. For example, the time mobile window considers three consecutive PPIs when the temporal aggregation lasts 10 minutes. If the pixel rainfall intensity values considered in this window are all valid and hold valid time intervals, the rainfall intensity value is determined as the arithmetic mean value in the same window. It then becomes necessary to establish some "threshold intensities" which allow to calculate the ARF depending on the return

period. The threshold intensities are values of heavy rainfall over the whole study area depending on duration and return period. Therefore, the intensity-duration (ID) curves of the annual maxima for the 6 recording raingauges indicated in Figure 7 were constructed towards this end. All raingauges had at least 30 years of annual maximum series and were arranged in such a way as to cover adequately the radar scanning region and the resultant annual data series were then analysed to obtain their frequency distributions.

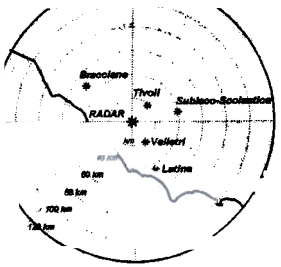

Figure 7. Location of selected raingauges in respect of the radar one

Finally, the rain intensities over the entire radar field of view were calculated for the prefixed 4 return periods (T = 2, 10, 25 and 50 years) and 5 durations (δ = 1, 5, 10, 60, 120 min). To a first approximation the arithmetic mean of the rain intensities was calculated per each duration and return period in order to evaluate one intensity value over the whole radar scanning region. In fact the areal average rainfall rates determined by using the Thiessen method are quite the same. Results are shown in Table 1.

At this point, it is possible to compare the values calculated per each considered duration with the relevant rainfall intensities determined by the arithmetic-mean method shown in Table 1.

Table 1. Rain intensity values (mm/h) over the whole radar scanning region

Arithmetic-mean method (A)					
T	i_1	i_5	i_{10}	i_{60}	i_{120}
2	133	103	82	31	19
10	206	160	128	48	30
25	243	189	150	57	35
50	271	210	167	63	39
Thiessen method (T)					
T	i_1	i_5	i_{10}	i_{60}	i_{120}
2	133	103	82	31	19
10	208	161	128	48	30
25	245	190	152	57	35
50	273	212	169	64	40
Percentage difference between A to T					
T	i_1	i_5	i_{10}	i_{60}	i_{120}
2	0.3	0.3	0.4	0.2	0.5
10	0.6	0.6	0.6	0.5	0.5
25	0.7	0.7	0.7	0.7	0.7
50	0.7	0.7	0.8	0.7	0.6

Actually, the values in Table 1 are assumed as threshold intensities allowing to computing the ARF depending on the return period. As a matter of fact, the only pixels over which the ARF is calculated

are those with an intensity higher than the said threshold intensity per each time aggregation and return period considered. In order to analyse the ARF trend when increasing the area, the size of the above-mentioned pixels were increased with an upscaling process until we had rainfall estimation over an area of 900 km^2 (see Figure 8). The rainfall intensity over each "increased" pixel is calculated as described above.

Finally, the trends of the 95th percentile of the ARF data sample with increasing area are shown in comparison with some of the most important empirical ARF-area relationships found in literature (see Figure 9):

Chow (1964) relation:

$$ARF = \left(1 + \frac{1.93A}{10^3}\right)^{-1} \quad (5)$$

Horton's relation, Various Authors (1990):

$$ARF = exp\left(-0.09 \cdot A^{0.23}\right) \quad (6)$$

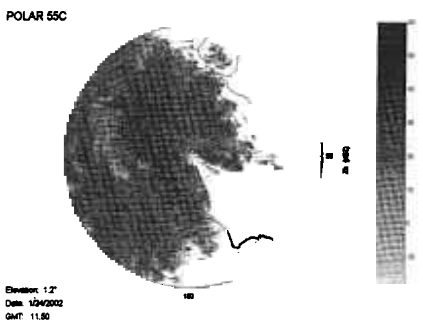

Figure 8. Size increasing process of a pixel

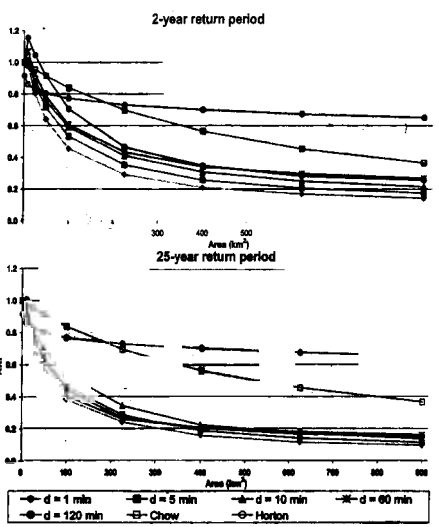

Figure 9. ARF trends with increasing area for various durations and return periods in comparison with some ARF-area literature relationships

It is evident that all of the empirical curves overestimate the ARF for large areas (A) and high durations, especially with increasing return period. But we wish to emphasise that empirical curves underestimate the ARF for small areas and return periods.

5. Conclusions

The results obtained show how the GDSTM model, calibrated on the study area, is able to forecast satisfactorily the rainfield in space and time. In calibrating the model, particular attention should be paid to the parameter estimation, since the minimisation of the objective function can lead to the identification of local minima with wrong mean values of rainfields. During the simulation, and especially when the model is applied in real time, it is necessary to consider adequately the inevitable transitory range of the simulated scenarios. The application of the model, coupled with a geo-morphological rainfall-runoff model, based on width function (WFIUH), obtained significant and very encouraging results for the forecasting of floods.

Furthermore, the study on the ARF seems to be quite important in floodplain management as well as in the design of urban drainage systems. As a matter of fact for small and medium size basins (200÷900 km^2), 25-year return periods, and 1÷2-hour concentration times, we estimate ARF ranging from 0.1 to 0.3 while empirical curves in literature estimate ARF ranging from 0.4 to 0.8, thus causing a remarkable overestimation of rainfall.

Also, the results lead to key consequences in hydrologic design for urban drainage systems. In fact small areas and return periods are usually considered in the design of urban drainage sewers. In these cases, the present work shows that no ARF ranging from 0 to 1 should be applied to point rainfall measurements, but the ARF should be definitely greater than 1 for catchments with high concentration times (> 1 h) in order to avoid underestimating rainfall and consequently the pipe lines.

In conclusion, in order to generalize the results obtained here the methodology should be applied to different geographical areas and climatological conditions.

6. Acknowledgements

The authors thank Dr. Eugenio Gorgucci of the Institute of Atmospheric Sciences and Climate of the National Research Council for interesting discussions and for providing the radar data. This research was partially supported by the National Group for Defence from Hydrogeological Hazards of the National Research Council (GNDCI-CNR, Italy).

7. References

Anagnostou, E.N. & Krajewski, W.F. 1999 Calibration of the WSR-88D precipitation processing subsystem. Weather Forecasting, Vol. 13, pp. 396-406.

Austin, P. & Houze, R. 1972 Analysis of the structure of precipitation patterns in New England. Journal of Applied Meteorology, Vol. 11, pp. 926-935.

Bastin, G., Lorent, B., Duque, C. & Gevers, M. 1984 Optimal estimation of the average rainfall and optimal selection of raingauge location. Water Resources Research, Vol. 28, pp. 1133-1144.

Borga, M., Anagnostou, N. & Frank, E. 2000 On the use of real-time radar rainfall estimates for flood prediction in mountainous basins. Journal of Geophysical Research, Vol. 105, pp. 2269-2280.

Bras, R.F. & Rodriguez-Iturbe, I. 1976 Network design for the estimation of areal mean rainfall events. Water Resources Research, Vol. 12 (6), pp. 1185-1195.

Chow, V. T. Handbook of Applied Hydrology, McGraw-Hill, New York, 1964.

Chua, S.H. & Bras, R.F. 1982 Optimal estimation of mean areal precipitation in regions of orographic influences. Journal of Hydrology, Vol. 57, pp. 713-728.

Cox, D. & Isham, V. 1988 A simple spatial-temporal model of rainfall. Proceeding of Royal Society

of London, Vol. A415, pp. 317-328.

Gorgucci, E., Scarchilli, G. & Chandrasekar, V. 1995 Radar and surface measurements of rainfall during CaPE. Journal of Applied Meteorology, Vol. 34, pp. 1570-1577.

Hansen, L.R. 1982 Large sample properties of generalized method of moments estimators. Econometrica, Vol. 50, pp. 1029-1054.

Lopez, V., Napolitano, F. & Russo, F. 2005 Calibration of a rainfall-runoff model using radar and raingauge data. Advances in Geosciences, Vol. 2, pp. 41-46.

Natural Environmental Research Council (NERC) Flood studies report, Vol. 2, Meteorological studies, Swindon, England, 1975.

Northrop, P.J. Modelling and statistical analysis of spatial-temporal rainfall fields, PhD thesis, Department of Statistical Science, University College London, 1996.

Rinehart R. E. Radar for meteorologists, Knight Printing Company, 1991.

Russo, F., Napolitano, F. & Gorgucci, E. 2005 Rainfall monitoring systems over an urban area: the city of Rome. Hydrological Processes, Vol. 19 (5), pp. 1007-1019.

Todini, E. 1995 The role of rainfall measurements and forecasts in real-time flood forecasting and management. Proceedings of the III International Symposium on Weather Radars, San Paulo, Brazil.

Various Authors Manuale di Ingegneria Civile, Zanichelli – Esac, Rome, 1990.

Waymire, E. & Gupta, V.K. 1981 The mathematical structure of rainfall representation: 1) A review of the stochastic rainfall models; 2) A review of the theory of point processes; 3) Some applications of the point process theory to rainfall processes. Water Resources Research, Vol. 17 (5), pp. 1261-1294.

Waymire, E., Gupta, V.K. & Rodriguez-Iturbe, I. 1984 A spectral theory of rainfall intensity at the meso-β scale. Water Resources Research, Vol. 20 (10), pp. 1453-1465.